Confined shocks inside isolated liquid volumes: A new path of erosion?

D. Obreschkow,[1] N. Dorsaz,[2] P. Kobel,[1] A. de Bosset,[1] M. Tinguely,[1] J. Field,[3] and M. Farhat[1]
[1]*EPFL, Laboratoire des Machines Hydrauliques, Av. Cour 33bis, Lausanne 1007, Switzerland*
[2]*Department of Chemistry, University of Cambridge, Cambridge CB2 1EW, United Kingdom*
[3]*Physics and Chemistry of Solids, Cavendish Laboratory, Cambridge CB3 OHE, United Kingdom*

(Received 25 June 2011; accepted 13 September 2011; published online 13 October 2011)

The unique confinement of shock waves inside *isolated* liquid volumes amplifies the density of shock–liquid interactions. We investigate this universal principle through an interdisciplinary study of shock-induced cavitation inside liquid volumes, isolated in 2 and 3 dimensions. By combining high-speed visualizations of ideal water drops realized in microgravity with smoothed particle simulations, we evidence strong shock-induced cavitation at the focus of the confined shocks. We extend this analysis to ground-observations of jets and drops using an analytic model and argue that cavitation caused by trapped shocks offers a distinct mechanism of erosion in high-speed impacts $(100\,\mathrm{ms}^{-1})$. © *2011 American Institute of Physics*. [doi:10.1063/1.3647583]

Shock waves in liquids are a common cause of cavitation,[1–5] in particular when shocks are reflected and focussed.[6] Famous examples include shock-induced cavitation in lithotripsy[7,8] and the "white crown" on the sea surface following an underwater detonation.[9–11] However, little is known about shock-induced cavitation inside "isolated" liquid volumes,[12] which are completely bounded by a free surface. The crucial feature of such systems is their unique confinement: the closed surface acts as a mirror trapping the shock and amplifying its local interaction with the fluid. Experimental hints for the importance of this mechanism for generating cavitation were provided by some of the earliest high-speed visualizations of shocked drops [Ref. 13, see reprint in Fig. 1(a)].

In this letter, we study the amplification of shock-induced cavitation in liquid volumes isolated in three dimensions (3D), such as drops, and in two dimensions (2D), such as jets. Illustrations of shock-driven cavitation in both cases are provided in Fig. 1. To understand this cavitation, we perform a systematic experimental study of shock-induced cavitation inside large, spherical water drops. These drops are realized in microgravity conditions aboard parabolic flights (European Space Agency, 42nd Parabolic Flight Campaign). In parallel to those experiments, we provide a quantitative explanation of the observed cavitation patterns through numerical simulations of dissipative shocks inside spheres and derive an analytic model to predict the location of shock-induced cavitation. Thereby, we demonstrate that shock-induced cavitation in isolated volumes is a universal phenomenon. Finally, we discuss a potential implication of cavitation caused by trapped shocks for drop erosion of solid surfaces.

Our microgravity experiment can be seen as an ideal laboratory for the study of shock dynamics inside stable drops. The setup [details in Ref. 15] can produce a spherical drop of demineralized water (diameter $D = 16$–26 mm). This drop is smoothly expelled through an injector tube, which also serves as a permanent attach-point for the drop (see Fig. 2, left). A movable pair of electrodes penetrating the drop from the top in Fig. 2 releases a fast (10 ns) discharge at a specific location within the drop. This discharge forms a supersonically expanding point-plasma [physics in Ref. 16], which generates a spherical shock wave and a vapor bubble,[17] called the "primary cavitation bubble." We here focus on the shock wave, while regarding the primary cavitation bubble as a welcome side-effect to estimate the energy of the shock wave. In fact, early studies of laser-induced point-plasmas[15,18] evidenced that the shock energy E_s approximately equals the bubble energy $E_\mathrm{b} = 4\pi/3 \cdot r_\mathrm{max}^3 \cdot (p_\infty - p_v)$, where r_max is the maximal bubble radius, $p_\infty = 80$ kPa is the static water pressure (= ambient pressure in the aircraft cabin), and $p_\mathrm{v} = 3.2$ kPa is the water vapour pressure at the working temperature $T \approx 25\,^\circ$C. Here, we study cases in the range $r_\mathrm{max} = 2$–4 mm; hence, $E_\mathrm{s} \approx E_\mathrm{b} \approx 3 - 20$ mJ. The fast phenomena produced by the shock are recorded using a high-speed camera (Photron Ultima APX) at up to 120 000 frames/sec and 50 μm spatial resolution.

The data is acquired in 36 microgravity cycles, each of 20 s duration. Each cycle allows us to generate a single water drop and to release one shock wave within this drop. The free parameters defining such a cycle are the drop diameter D, the shock energy E_s, and the location of the shock center. The latter is expressed by the eccentricity $\varepsilon \equiv s/(D/2) \in [0, 1]$, where s is the distance between the drop center and the shock center. The results presented in this letter rely on the 18 parameter configurations corresponding to all possible combinations of $D \in \{16\text{ mm}, 22\text{ mm}\}$, $E_s \in \{3\text{ mJ}, 10\text{ mJ}, 20\text{ mJ}\}$, and $\varepsilon \in \{0.2, 0.4, 0.6\}$. Each configuration is repeated twice to verify the repeatability of the data.

All 36 high-speed visualizations exhibit the same dominant feature: About 10 μs after the shock generation thousands of submillimetric bubbles appear synchronously in the hemisphere opposite the origin of the shock (Fig. 2, left).

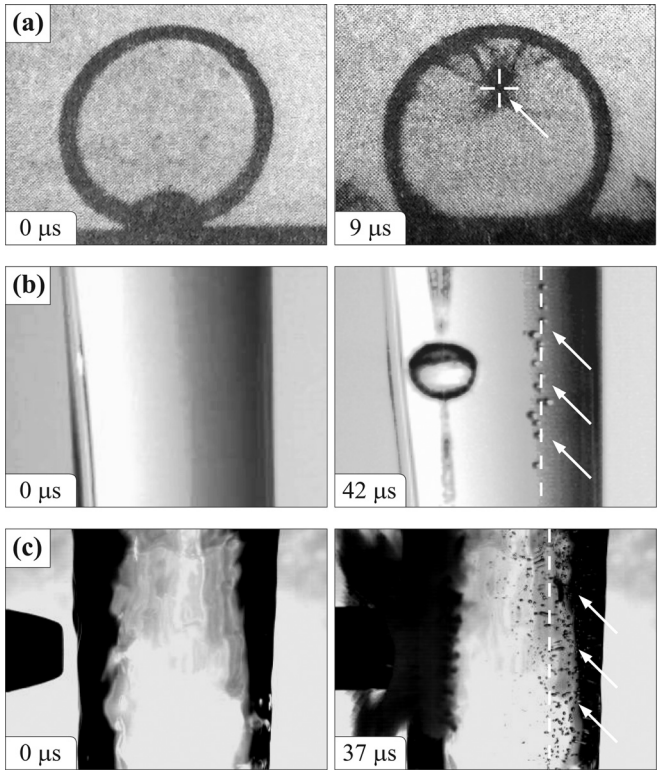

FIG. 1. Examples of cavitation (arrows) produced by reflected shock waves. (a) Liquid drop (88% water, 12% gelatine, diameter $D = 10$ mm) impacting on a hard solid surface at $v = 110$ ms^{-1} [reprinted with permission from J. E. Field, J. P. Dear, and J. E. Ogren, J. Appl. Phys. **65**, 533 (1989); copyright 1989, American Institute of Physics]; (b) Water jet ($D = 6$ mm) shocked by a laser pulse (energy = 30 mJ) on the left side [setup explained in Ref. 14]; (c) Water jet ($D = 22$ mm) impacted by a 9 mm-projectile at $v = 200$ ms^{-1} [collaboration with the Swiss army]. Dashed lines indicate the position, where the cavitation should occur according to Eq. (2), corrected for optical refraction (Ref. 15).

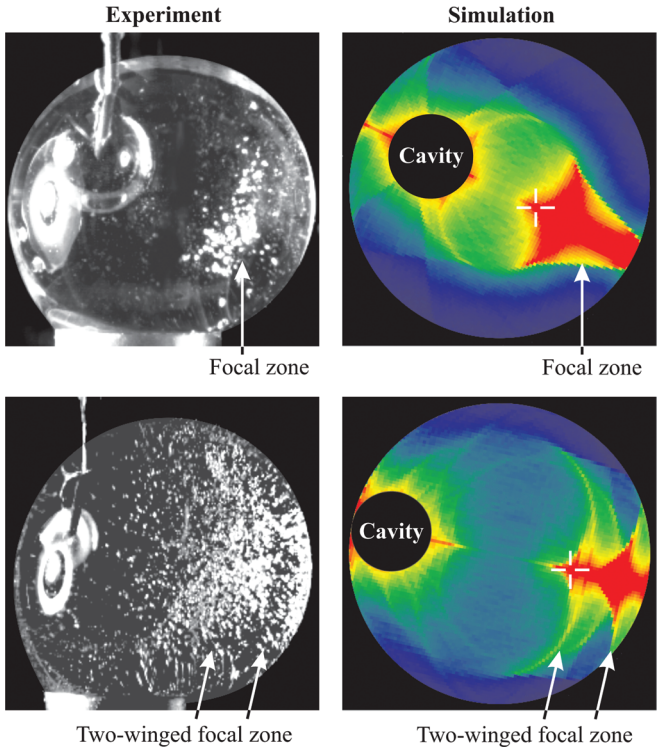

FIG. 2. (Color) Spherical water drop ($D = 22$ mm) 80 μs after the generation of a spherical shock at the location labelled "cavity" (since here the primary cavitation bubble forms in the case of a plasma-driven shock). Left images show the observed shock-induced cavitation, while the right images are simulated counter-parts; the colors range from lowest (blue) to highest (red) energy density. The eccentricities of the shock origins are $\varepsilon = 0.4$ (upper) and $\varepsilon = 0.6$ (lower), though they appear to be larger due to optical refraction [refraction model in Ref. 15]. Dashed crosses indicate where the strongest cavitation should occur according to Eq. (2).

The fastest visualizations (120 000 frames/sec) uncover that these micro-bubbles grow and collapse, their longest life-times lying around 50 μs. This transient behavior and the coherent formation of the bubbles at the instant of the shock transition disclose that the bubbles are a form of shock wave-induced cavitation[1–4,19,20]—a phenomenon known as "secondary cavitation" in other situations. The largest bubbles have diameters of $d \approx 0.5$ mm, which in the Rayleigh-model[21] of spherical cavitation bubbles implies life-times of $t_R = 0.915d[\rho/(p_\infty - p_v)]^{1/2} \approx 50$ μs, consistent with our observations.

The discrepancy between the high bubble-density seen in Fig. 2 (left) and the faint traces detected by others[2] can be explained by the particular confinement of our shock. The free drop surface causes an elastic reflection of a pressure wave; hence, the shock bounces back and forth while successively dissipating its energy to shock-induced cavities. To check if the full shock energy is converted into cavitation bubbles, we estimate the total volume V of these bubbles from their radii (corrected for optical refraction by using our optical model in Ref. 15). The implied energy $E = V \cdot (p_\infty - p_v)$ is systematically consistent (within 20% measurement uncertainties) with the original shock energy E_s.

Depending on the experimental parameters, the cloud of shock-induced bubbles appears in different intensities and geometries (Fig. 2). A systematic investigation of all samples uncovers that the intensity (size and number) of bubbles varies with the shock energy E_s and drop diameter D. In return, the geometry of the bubble-cloud exclusively depends on the eccentricity ε. To understand this dependence on ε, we consider the shock as a spherical shell that isotropically expands from a single point specified by ε. This shell is represented by $N = 10^5$ particles, which initially propagate on straight lines at the speed of sound $c = 1500$ ms^{-1}. When reaching the drop surface, they are reflected elastically. Each particle carries a shock energy $E_p(t) \propto (\delta p)^2$, where δp is the pressure fluctuation relative to the equilibrium state. (Note that δp changes its sign when reflecting at the free surface, while the energy remains unchanged.) As these "shock quanta" propagate across the liquid, they form cavitation via evaporation in the tensile case ($\delta p < 0$) or through forcing the collapse and subsequent rebound of existing nuclei in the compressive case ($\delta p > 0$). In both cases, the generation of cavitation bubbles decreases the energy of the shock by decreasing $|\delta p|$. We assume that this decrease in energy happens at a constant fraction per unit time (independently of the sign of δp), as typical for most dissipative processes. Thus, $E_p(t) = E_s/N \cdot \exp(-t/\tau)$, where τ is the time in which the shock dissipates $(1 - 1/e) \approx 63\%$ of its energy. Here, we choose $\tau = 20$ μs since the shock-induced bubbles in Fig. 2 (left) reach an integrated potential energy, measured through the bubble sizes, of $(0.6 \pm 0.2)E_s$ within 20 μs. The

simulation progresses at a discrete time step $\mathrm{d}t = 10^{-8}$ s, chosen sufficiently small to obtain converging results. In each step and for each particle, the dissipated energy $|\mathrm{d}E_\mathrm{p}(t)| = -\dot{E}_\mathrm{p}\,\mathrm{d}t$ is transcribed to the liquid at the location of the particle using a 3D Gaussian smoothing kernel with a variance equal to the mean separation between neighboring particles. To tackle the energy acquired at different locations in the drop, the latter is discretized on a regular mesh of $256^3 \approx 1.7 \cdot 10^7$ cubic cells.

The output of these numerical simulations is a 3D density map of the energy dissipated by a spherical shock trapped inside a spherical drop. To compare these maps against the 2D images of shock-induced cavitation inside drops, the simulated maps were projected onto a plane, while accounting for the optical refraction at the water surface [according to our model in Ref. 15]. Figure 2 compares the simulation against the observations for the two eccentricities $\varepsilon = 0.4, 0.6$. The patterns of the simulated energy density and the observed shock-induced cavitation exhibit remarkable similarities in both cases: (i) the highest densities appear opposite the origin of the shock wave at a comparable eccentricity and (ii) for high eccentricities $(\varepsilon > 0.5)$, the bubble-patterns spread out in two wings. This match between simulation and experiment confirms that the patterns of shock-induced cavitation can be understood in terms of reflected dissipative waves.

Can we then analytically understand the observed and simulated patterns of shock-induced cavitation? Due to axial symmetry, the 3D geometry of a spherical wave inside a sphere can be reduced to a 2D circular wave reflected inside a circle (Fig. 3). Unlike ellipses, circles yield no focal point for an eccentric circular wave. Instead, the reflected rays are concentrated within a zone enveloped by the "catacaustic" (dashed line in Fig. 3), defined as the location where reflected rays intersect. On this catacaustic, we expect a high density of the reflected shock. This model can be extended to 3D by performing a rotation about the axis of symmetry (horizontal axis in Fig. 3). Doing so, we introduce an additional $1/r$-factor in the shock density, where r is the distance from the axis of symmetry. Thus, the location of the highest density of shock-induced cavitation is defined by the intersection of the catacaustic and the axis of symmetry. This intersection lies at a position μ (see Fig. 3) that depends on the wave origin $\varepsilon \in [0, 1]$. To express μ as a function of ε, consider a single ray emitted at an angle $\alpha\ \varepsilon\ (0, 2\pi)$ and crossing the center line at the position x after its reflection (thick line in Fig. 3). From the law-of-sines, $\sin(\beta/2) = \varepsilon \sin\alpha$ and $\sin(\beta/2) = -x \sin\gamma$, and trivially $\alpha + \beta + \gamma = \pi$, which solve to

$$x = \frac{-\varepsilon \sin\alpha}{\sin[\alpha + 2\arcsin(\varepsilon \sin\alpha)]}. \tag{1}$$

Equation (1) is meaningful if $x\ \varepsilon\ [-1, 0]$, while, otherwise, the ray is reflected more than once before crossing the center line. For any $\varepsilon \in [0, 1]$, the maximum $\mu \equiv \max\{x(\varepsilon, \alpha) \in [-1, 0]\}$ is reached as $\alpha \to 0$; thus

$$\mu = -\varepsilon/(2\varepsilon + 1). \tag{2}$$

In conclusion, Eq. (2) specifies the location of strongest shock-induced cavitation. This prediction fits the observations (see crosses and lines in Figs. 1 and 2).

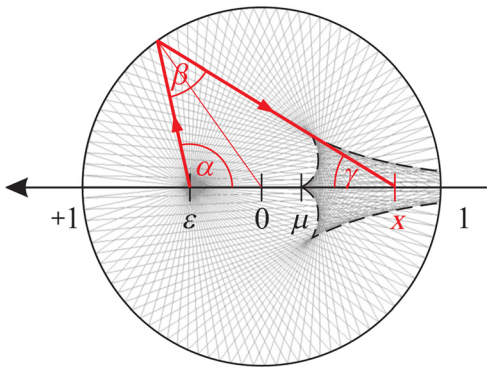

FIG. 3. (Color online) Circular wave reflected inside a circle. The thick line highlights a selected path. The ensemble of all reflected paths defines the dashed envelope called "catacaustic." This envelope has a peak point μ that depends on the wave origin ε via Eq. (2). Here, $\varepsilon = 0.4$ as in Fig. 2 (top).

We finally wonder about the erosive potential of the cavitation induced by reflected shocks. In Fig. 1(c) the impact of the projectile is fast enough for the cavitation bubbles to survive until the projectile reaches them. This suggests that fast liquid-solid collisions may also cause erosion via shock-induced cavitation at the far-side of the impact point. To calculate the required impact velocity for a drop with diameter D (e.g., a rain drop), we assume that a spherical shock wave is emitted at the initial contact point. Hence, the strongest shock-induced cavitation is located at a distance $2D/3$ from the contact point [Eq. (2) with $\varepsilon = 1$]. The reflected shock reaches this focus at a time $t_\mathrm{c} \approx 4D/(3c)$ after the impact, where c is the speed of sound, while the impacting solid itself reaches the same point at a time $t_\mathrm{v} \approx 2D/(3v)$, where v is the impact velocity. For erosion to take place, we, therefore, require $t_\mathrm{c} + t_\mathrm{R} \geq t_\mathrm{v}$, where t_R is the life-time of the bubbles.[21] Hence, a lower impact velocity limit for this type of erosion is

$$v \geq \left(\frac{3\,t_\mathrm{R}}{2D} + \frac{2}{c}\right)^{-1}. \tag{3}$$

Equation (3) is valid for $2v < c$ since, otherwise, the solid reaches the shock focus before the reflected shock itself. The characteristic bubble life-time t_R depends on the liquid and shock parameters, although our cases (Figs. 2, 1(b), and 1(c)) all yield average life times of order $t_\mathrm{R} = 20\ \mu$s (with the highest values reaching $t_\mathrm{R} = 50\ \mu$s). Adopting $t_\mathrm{R} = 20\ \mu$s for the case of a typical rain drop ($D = 3$–4 mm, $c \approx 1500$ ms^{-1}), Eq. (3) then gives a lower velocity limit of $v \approx 100$ ms^{-1}, which is roughly an order of magnitude above the free fall velocity of rain. This reveals that the mechanism of cavitation erosion described in this section will only be active in particular cases, such as aircrafts and missiles eroded by rain[22,23] and Pelton turbine blades eroded by high-speed (up to 200 ms^{-1}) droplets and jets.[24]

Fig. 4 presents a synthetic view of the most important mechanisms of erosion that are known to occur during the impact of a liquid drop:

(a) *Hammer pressure:* On initial contact, erosion can result from the high compression-pressure of up to $p = 3\rho cv$ for rigid solids,[13] which exists while the contact edge expands supersonically.

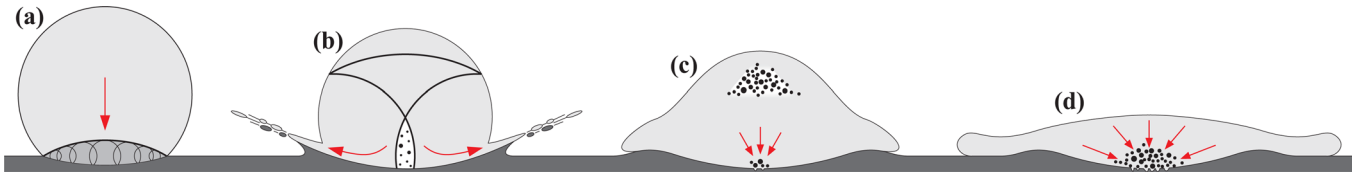

FIG. 4. (Color online) Four mechanisms of erosion by an impacting liquid drop (see main text). The last mechanism is proposed in this letter. The conditions for these mechanisms differ; hence, only some of them may affect a particular impact.

(b) *Jetting:* When the contact edge becomes subsonic, the pressure-shock detaches from the contact edge and high-speed jets emerge from the latter,[13] causing shear erosion[25] (e.g., crater rims formed by hypersonic impacts of atoms[26] and meteorites[27]).
(c) *Near-side cavitation:* A lateral pressure shock travelling from the contact edge to the axis of symmetry can produce cavitation next to the initial contact point,[28,29] which may cause point-like erosion.[30]
(d) *Far-side cavitation:* New mechanism suggested here, which occurs via cavitation caused by reflected shocks opposite the impact point (see also simulations of low pressure at the shock-focus[31–33]).

We emphasize that a particular drop impact may only involve some of these erosive mechanisms. A systematic study of the applicability of each mechanism as a function of dynamical and geometrical parameters as well as material properties promises an interesting road for forthcoming research.

This research was supported by the Swiss National Science Foundation (Grant Nos. 200020-116641, PBELP2-130895) and the European Space Agency ESA. We thank E. Robert, M. Rouvinez, and the Swiss Army for contributing to the images in Figs. 1(b) and 1(c).

[1]V. K. Kedrinskii, "Shock induced cavitation," in *Shock Wave Science and Technology Reference Library*, edited by M. E. H. van Dongen (Springer, Berlin, Heidelberg, 2007), pp. 67–97.
[2]Y. Tomita, T. Kodama, and A. Shima, "Secondary cavitation due to interaction of a collapsing bubble with a rising free surface," Appl. Phys. Lett. **59**(3), 274 (1991).
[3]L. C. Hagenson and L. K. Doraiswamy, "Comparison of the effects of ultrasound and mechanical agitation on a reacting solid-liquid system," Chem. Eng. Sci. **53**(1), 131 (1998).
[4]B. Wolfrum, T. Kurz, R. Mettin, and W. Lauterborn, "Shock wave induced interaction of microbubbles and boundaries," Phys. Fluids **15**(10), 2916 (2003).
[5]G. N. Sankin, W. N. Simmons, S. L. Zhu, and P. Zhong, "Shock wave interaction with laser-generated single bubbles," Phys. Rev. Lett. **95**(3), 034501 (2005).
[6]O. Lindau and W. Lauterborn, "Cinematographic observation of the collapse and rebound of a laser-produced cavitation bubble near a wall," J. Fluid Mech. **479**, 327 (2003).
[7]Y. Tomita, T. Obara, K. Takayama, and M. Kuwahara, "Cavitation phenomena in extracorporeal microexplosion lithotripsy," Shock Waves **3**, 149 (1994).
[8]T. G. Leighton and R. O. Cleveland, "Lithotripsy," Proc. Inst. Mech. Eng., Part H **224**(2), 317 (2010).
[9]E. B. Wilson, "Cavitation produced by shock waves in sea water," Phys. Rev. **72**(2), 178 (1947).
[10]R. P. Chapman and H. D. Scott, "Cavitation caused by explosive shock pulses reflected from the sea surface," J. Acoust. Soc. Am. **38**(5), 933 (1965).
[11]R. A. Wentzell, "Cavitation due to reflected shock pulses," J. Acoust. Soc. Am. **46**(1P1), 111 (1969).
[12]L. Heijnen, P. A. Quinto-Su, X. Zhao, and C. D. Ohl, "Cavitation within a droplet," Phys. Fluids **21**(9), 091102 (2009).
[13]J. E. Field, J. P. Dear, and J. E. Ogren, "The effects of target compliance on liquid drop impact," J. Appl. Phys. **65**(2), 533 (1989).
[14]E. Robert, J. Lettry, M. Farhat, P. A. Monkewitz, and F. Avellan, "Cavitation bubble behavior inside a liquid jet," Phys. Fluids **19**, 067106 (2007).
[15]Ph. Kobel, D. Obreschkow, N. Dorsaz, A. De Bosset, and M. Farhat, "Techniques for generating centimetric drops in microgravity and application to cavitation studies," Exp. Fluids **47**, 39 (2009).
[16]P. Kennedy, "Laser-induced breakdown in aqueous media," Prog. Quantum Electron. **21**, 155 (1997).
[17]D. Obreschkow, Ph. Kobel, N. Dorsaz, A. De Bosset, C. Nicollier, and F. Farhat, "Cavitation bubble collapse inside liquid spheres in microgravity," Phys. Rev. Lett. **97**(9), 094502 (2006).
[18]A. Vogel, S. Busch, and U. Parlitz, "Shock wave emission and cavitation bubble generation by picosecond and nanosecond optical breakdown in water," J. Acoust. Soc. Am. **100**(1), 148 (1996).
[19]M. Arora, C. D. Ohl, and D. Lohse, "Effect of nuclei concentration on cavitation cluster dynamics," J. Acoust. Soc. Am. **121**(6), 3432 (2007).
[20]T. G. Leighton, A. J. Walton, and J. E. Field, "High-speed photography of transient excitation," Ultrasonics **27**(6), 370 (1989).
[21]L. Rayleigh, "On the pressure developed in a liquid during the collapse of a spherical cavity," Philos. Mag. **34**, 94 (1917).
[22]A. A. Fyall, "Practical aspects of rain erosion of aircraft and missiles," Philos. Trans. R. Soc. London, Ser. A **260**(1110), 161 (1966).
[23]J. Zahavi, S. Nadiv, and G. F. Schmitt, "Indirect damage in composite materials due to raindrop impact," Wear **72**(3), 305 (1981).
[24]A. Perrig, "Hydrodynamics of the free surface flow in Pelton turbine buckets," Ph.D. thesis (EPFL, Switzerland, 2007).
[25]G. S. Springer, *Erosion by Liquid Impact* (Scripta, Washington, 1976), ISBN: 0470151080.
[26]J. Samela and K. Nordlund, "Atomistic simulation of the transition from atomistic to macroscopic cratering," Phys. Rev. Lett. **101**(2), 027601 (2008).
[27]L. E. Senft and S. T. Stewart, "Impact crater formation in icy layered terrains on Mars," Meteorit. Planet. Sci. **43**, 1993 (2008).
[28]J. E. Field, M. B. Lesser, and J. P. Dear, "Studies of two-dimensional liquid-wedge impact and their relevance to liquid-drop impact problems," Proc. R. Soc. London, Ser. A **401**(1821), 225 (1985).
[29]N. K. Bourne, T. Obara, and J. E. Field, "The impact and penetration of a water surface by a liquid jet," Proc. R. Soc. London, Ser. A **452**(1949), 1497 (1996).
[30]N. K. Bourne and J. E. Field, "A high-speed photographic study of cavitation damage," J. Appl. Phys. **78**(7), 4423 (1995).
[31]K. K. Haller, Y. Ventikos, D. Poulikakos, and P. Monkewitz, "Computational study of high-speed liquid droplet impact," J. Appl. Phys. **92**, 2821 (2002).
[32]T. Sanada, M. Watanabe, M. Shirota, M. Yamase, and T. Saito, "Impact of high-speed steam-droplet spray on solid surface," Fluid Dyn. Res. **40**(7-8), 627 (2008).
[33]J. Xiong, S. Koshizuka, and M. Sakai, "Numerical analysis of droplet impingement using the moving particle semi-implicit method," J. Nucl. Sci. Technol. **47**(3), 314 (2010).